Challenges in estimation of plot-scale emissivity and surface temperature using flux tower measurements

Gitanjali Thakur[1,*]**, Stanislaus J. Schymanski**[1]**, Kaniska Mallick** [1]**, Ivonne Trebs**[1]**, and Mauro Sulis**[1]

[1]Luxembourg Institute of Science and Technology, ERIN, Belvaux, L-4422, Luxembourg
[*]gitanjali.thakur@list.lu

ABSTRACT

Land surface temperature (LST) is a pre-eminent state variable that controls the energy and water exchange between the Earth's surface and the atmosphere. At landscape scale, LST is derived from thermal infrared radiance measured using space-borne radiometers. At the plot-scale, flux tower recorded longwave radiation components is inverted to retrieve LST. Since down-welling longwave component was not measured routinely for a long time a conventional practice is using stephan boltzmanfor the plot-scale LST retrieval (only up-welling longwave component) . This gives rise to the question if ignoring down-welling longwave radiation is adequate for plot-scale LST estimations. Another associated question is how to obtain the correct surface emissivity using flux tower measurement needed for plot-scale LST retrievals . The current work addresses these two important questions using observations at ten eddy covariance towers having different land cover types. We found that the LST values obtained using up-welling and down-welling longwave component (long equation) are 0.5 to 1.5K lower than if only up-welling longwave components were used (short equation). Plot-scale emissivity was estimated using observed sensible heat flux and estimated surface to air temperature difference. Plot-scale emissivity obtained using the complete equation was generally lower than if the simplified equation was used, for all land cover types. We also quantified the uncertainty in plot-scale LST and emissivity due to error in measured fluxes. We found that despite additional input data for the long equation, the uncertainty in plot-scale LST was not greater than if long equation was used. Landscape-scale day-time LST obtained from satellite data (MODIS TERRA) were strongly correlated with our plot-scale estimates, but on average higher by several degrees, regardless of the method of estimation. For most sites, the correspondence between MODIS LST and plot-scale LST estimates increased significantly if plot-scale emissivity was used instead of the landscape-scale emissivity obtained from satellite measurements. The implication of this work at ecosystem-scale (eddy covariance sites) can give an idea about the suitability of using aerodynamic and radiometric measurement in a common context (plot-scale emissivity estimation).

Introduction

The surface energy balance (SEB) can be sub-divided into radiative components (often lumped in net radiation, R_{net}) and thermodynamic components, including sensible, latent heat flux (H, LE respectively) and ground heat flux (G):

$$R_{net} = H + LE + G \tag{1}$$

In this text, all energy balance components are expressed as power per horizontal surface area, in (Wm^{-2}). As the surface to air temperature difference drives the exchange of sensible heat between surface and atmosphere, all components of Eq. (1) depend on the land surface temperature (LST). It directly affects the amount of emitted longwave radiation and it influences the saturation vapor pressure at the surface that drives latent heat flux. Thus, the ecohydrological functioning and carbon-water coupling are largely controlled by the surface temperature of the soil-vegetation system[1]. As it contains imprints of surface moisture variations and micro-climatic conditions within and above plant canopies, thereby controlling the magnitude and partitioning of the water and energy fluxes[2]. This makes LST of great importance to the modelling community. It is used to constrain climate models and weather prediction models[3,4], as a prognostic variable in land surface models (LSM) and as diagnostic variable in surface energy balance models[2,4]. Therefore, it is crucial to have access to reliable estimates of LST over large spatial and temporal scales.

Net radiation (R_{net}) can be sub-divided into down-welling and up-welling components. Only a fraction of solar top-of-the-atmosphere radiation reaches the Earth's surface, as some is reflected back to space by clouds, some is absorbed by the atmosphere and emitted later as longwave radiation. Part of the longwave radiation emitted by the atmosphere reaches the surface as down-welling longwave radiation (R_{ldown}), along with the remaining down-welling shortwave radiation (R_{sdown}). At the surface, parts of down-welling shortwave and longwave radiation are reflected back to the atmosphere (R_{sref} and R_{lref},

respectively), and the rest is absorbed. In addition to reflecting radiation, the surface is also emitting longwave radiation as a function of surface temperature (T_s, K) and surface emissivity (ε) following the Stefan-Boltzmann (SB) equation:

$$R_{lem} = \varepsilon \sigma T_s^4 \tag{2}$$

where σ ($Wm^{-2}K^{-4}$) is the SB constant. Putting the radiative components together, we can sub-divide R_{net} into:

$$R_{net} = R_{sdwn} + R_{ldwn} - R_{sref} - R_{lref} - R_{lem} \tag{3}$$

Reflected shortwave in Eq. (3) is can be expressed as $R_{sref} = \alpha R_{sdown}$, where α is the surface albedo. Similarly, reflected longwave is a function of down-welling longwave and surface emissivity (ε) and expressed as:

$$R_{lref} = (1 - \varepsilon)R_{ldwn} \tag{4}$$

LST or radiometric temperature can be estimated from the infrared radiance emanating from a given surface[5]. The emitted and down-welling longwave radiance are measured by an infrared radiometer at given angle within its instantaneous field of view (fov). The radiation received by a pyrgeometer or infrared sensor is a combination of the radiation emitted and reflected by the surfaces in the field of view. Thus, LST estimated from an infrared measurement is the "ensemble directional radiometric surface temperature", representing the ensemble of various surface elements present within the sensor's instantaneous fov[6]. A downward facing sensor relatively close to the surface (a few meters for an eddy covariance tower) essentially measures up-welling longwave radiation (R_{lup}) from the surface, which is the sum of emitted and reflected longwave radiation:

$$R_{lup} = R_{lem} + R_{lref} \tag{5}$$

Substitution of Eqs. 4 and 2 into Eq. 5 yields R_{lup} as a function of emissivity, surface temperature and down-welling longwave radiation:

$$R_{lup} = \varepsilon \sigma T_s^4 + (1 - \varepsilon)R_{ldwn} \tag{6}$$

The above equation can be solved for surface temperature as a function of measured longwave and known surface emissivity:

$$T_s = \sqrt[4]{\frac{R_{ldwn}}{\sigma} - \frac{R_{ldwn}}{\varepsilon \sigma} + \frac{R_{lup}}{\varepsilon \sigma}} \tag{7}$$

where, ε is the surface emissivity ranging between 0 and 1, σ ($Wm^{-2}K^{-4}$) is the Stefan-Boltzman constant and T_s (K) is the LST. Emissivity is defined as efficiency of a surface to emit thermal energy relative to a perfect black body. It depends on surface morphology, soil moisture, soil chemistry, roughness, spectral wavelength, temperature and view angle[6]. The radiative energy emitted at a specific wavelength is related to its temperature using Planck's function[7]. The emissivity of a land surface (composed of various grey body) is retrieved using radiative transfer models[8–10]. Thermal remote sensing (MODIS) is used to measure spectral emissivity through four channels (28, 29, 30, 31) at wavelengths ranging between 8-12 μm[11] and the system of equations iteratively solved for a given range of wavelengths (9 - 12μm) to obtain ε and LST.

In last two decades, plot-scale radiometric data collected at eddy covariance sites (ECS) have gained popularity for in-situ LST retrieval due to its high spatial and temporal resolution. In addition to this the land cover specificity is also an important factor as the LST estimates are of relatively homogeneous footprint in comparison to MODIS pixels. These measurements are primarily use to assess the impacts and feedbacks of climate change on key ecosystem fluxes[12]. In order to invert LST as shown in Eq. (7), ε values are required. However, the surface emissivity of the tower footprint cannot be estimated using radiative transfer models as radiometers do not measure spectral bands separately to deduce emissivity directly.

By definition, LST is a thermodynamic temperature that can be felt or measured by an accurate thermometer at the land surface-atmosphere point-of-contact and is independent of wavelength[13]. The instantaneous value of LST is the result of interplay between the net radiation at the surface, ground heat flux and turbulent fluxes of heat (H) and moisture (LE)[14]. Thus, LST can also be used for the estimation of the sensible heat flux[15] and latent heat flux[16] between the surface and the atmosphere. For plot-scale emissivity retrieval we focus on H, which is defined as heat transfer driven by a surface to air temperature difference. It can be expressed mathematically in analogy to Ohm's law as:

$$H = \rho C_p (T_s - T_a)/r_a \tag{8}$$

$$H = m(T_s - T_a) \tag{9}$$

where T_a (K) is the temperature of the air measured at some height above the surface, $C_p(Jkg^{-1}K^{-1})$ is the specific heat capacity of air, $\rho(kg(m)^{-3})$ is the air-density, $r_a(Sm^{-1})$ is the total resistance to heat transport from surface to the atmosphere. $m(m/s)$ is a proportionality constant obtained by lumping $(\rho C_p/r_a)$ and can be broadly referred as heat transfer coefficient. m depends on surface characteristics and micro meteorology[17]. It is evident from Eq. (9), that for $T_s - T_a = 0$ (ΔT=0), H will be zero. This boundary condition and the linearity of H and ΔT relationship is used to estimate ε at the plot scale from observed of H, T_a and estimated T_s using measured longwave[18-20].

However, due to surface heterogenity sparse canopy is prone to footprint mismatch between the aerodynamic (flux tower) footprint and radiometric (hemispherical) footprint[21-23] which can result into a different boundary condition i.e at $\Delta T = 0, H \neq 0$. Aerodynamic footprint represents the area contributing to measured sensible heat, air temperature and the hemispherical footprint is the area within radiometric FOV contributing to the measured longwave (used for T_s estimation). For instance if the radiometer fov has more tree crowns and less soil in comparison to the flux tower footprint the observed longwave will have a bias. In this kind of scenario we would expect a non zero H for 0 ΔT. In order to capture such a bias in plot-scale ε estimation we allowed $H(\Delta T)$ linear regression to have an intercept (c) as shown in Eq. 10.

$$H = m(T_s - T_a) \pm c(H) \tag{10}$$

H is representative of the sensible heat flux from eddy covariance tower footprint,T_s is representative of all the radiating surfaces in the sensor's view. C is interpreted as the H from aerodynamic footprint which is not seen by the radiometer. For example if the mismatch in footprint is a hotter area relative to the shared foot print of the measuring devices i.e. dry soil patch then $H(\Delta T)$ relationship can be represented by adding a negative intercept to the $H(\Delta T)$ relationship. Similarly if the footprint mismatch is a relatively colder area i.e leaves in shade the regression can have a positive intercept.

Plot-scale ε estimation using observed H, T_a, R_{lup}, R_{ldw} as described above, may be fraught with substantial uncertainty. As it is unclear how error in observed fluxes propagates into the uncertainty of estimated LST and ε. The turbulent fluxes of H measured at the ECS are averaged over smaller time (30 or 60 minutes) and the averaging over this time interval is typically dominated by random errors[24,25]. The other source of error is the radiation measurement which can vary between sites, due to the difference in accuracy and precision of the in-situ radiometers or pyrgeometer, differences in field of view (FOV), wavelength bands, and spectral response functions of the sensors. For reference, the accuracy of dedicated infrared temperature (IRT) sensors is given by their manufacturers as 0.5K, but it is not clear what sources of uncertainty are considered in this estimation[26]. By design, IRT sensors only measure upwelling infrared radiance and therefore cannot explicitly account for the amount of reflected down-welling infrared radiation in the signal. For a long time, down-welling longwave R_{ldw} was not routinely observed at ECS[27] and was also considered to be the most poorly quantified component of the radiation budget[28]. Therefore, the second term in Eq. (6) is commonly omitted, arguing that $\varepsilon \approx 1$, and therefore Eq. (6) is simplified to[29]:

$$R_{lup} \approx \varepsilon \sigma T_s^4 \tag{11}$$

Eq. 11 can be solved for T_s to yield what we will term the "short equation" (SEQ) for T_s:

$$T_s \approx \sqrt[4]{\frac{R_{lup}}{\varepsilon \sigma}} \tag{12}$$

Note that the above derivation is actually flawed, as the second term of Eq. (6) was omitted arguing that $\varepsilon \approx 1$, and yet ε was retained in the first part of the equation. Nevertheless, even with the availability of down-welling longwave measurements[30], the use of Eq. (11) is still a common practice[31]. This gives rise to the question if the short equation (Eq. 12) is adequate to estimate LST from ground-based measurements. In the remainder of this paper, we will refer to LST obtained using the complete or "long equation" (Eq. 7) as T_{leq} and to LST obtained using the simplified or short equation (Eq. 12) as T_{seq}.

In the present study, we evaluate and analyse the differences in plot-scale LST and emissivity estimated using the complete (Eq. 7) and short (Eq. 12) equations. The following research questions are addressed:

1. Is the short equation (Eq. 12), neglecting the reflected down-welling longwave radiation, adequate to estimate LST from ground-based measurements?

2. Does the estimation of plot-scale ε based on observed sensible heat flux H has an advantage over satellite derived ε for LST estimation?

3. How much uncertainity is introduced in plot-scale LST and ε due to errors in measured fluxes?

To answer these questions, we analysed data for 10 eddy covariance sites in different biomes and climates (see Table 2). Plot-scale broadband monthly emissivity was derived using observed H and estimated ΔT as proposed by Holmes et al.[18].

Plot-scale LST was estimated using plot-scale or landscape-scale emissivity with (Eq. 7) and (Eq. 12). Plot-scale LST were compared with MODIS LST (TERRA satellite-sensed) for the times of satellite over-pass. Uncertainty in emissivity and LST due to error in observed fluxes was calculated using SOBOL based uncertainty analysis (SAlib)[32]. See the Methods section for more details.

1 Results

1.1 Plot-scale ε using complete and simplified equation

Following the method proposed by Holmes et al.[18,33], plot-scale monthly emissivity (ε) was estimated at the study site by fitting ε to minimise the root mean square error (RMSE) of the regression between H and $\Delta T = T_s - T_a$ for every month using filtered measurements (based on net radiation and wind speed). In Fig. 1a, c, and d, we reproduced the original data of Figs. 2a, 3C, and 3Q in Holmes et al. (2009)[18] to validate our interpretation of their approach using the simplified equation (Eq. 12). We noted only marginal differences between the two results based on the short equation which are likely due to data filtering and fitting algorithms. The replication of the $H(\Delta T)$ plot using the complete equation (Eq. 7) in their analysis is given in Fig. 1b. The use of complete equation (Eq. 7) resulted in substantially lower values of ε (10%) as compared the values estimated by Holmes et al[18] for the common study sites (Brookings, Yatir Forest) (Fig. 1c and d). Note that the complete equation also yielded $H(\Delta T)$ relationship for many more months at Yatir Forest than the short equation (Fig. 1d), as it resulted in achieving a strong correlation between H and ΔT, which is one of the filtering criteria for the approach. The retrieved LST values were slightly higher (compare Panels a and b in Fig. 1). The pattern of low ε and high LST using the complete equation compared to the simplified equation was confirmed for all 10 sites used in the present study (Table **SI 2**).
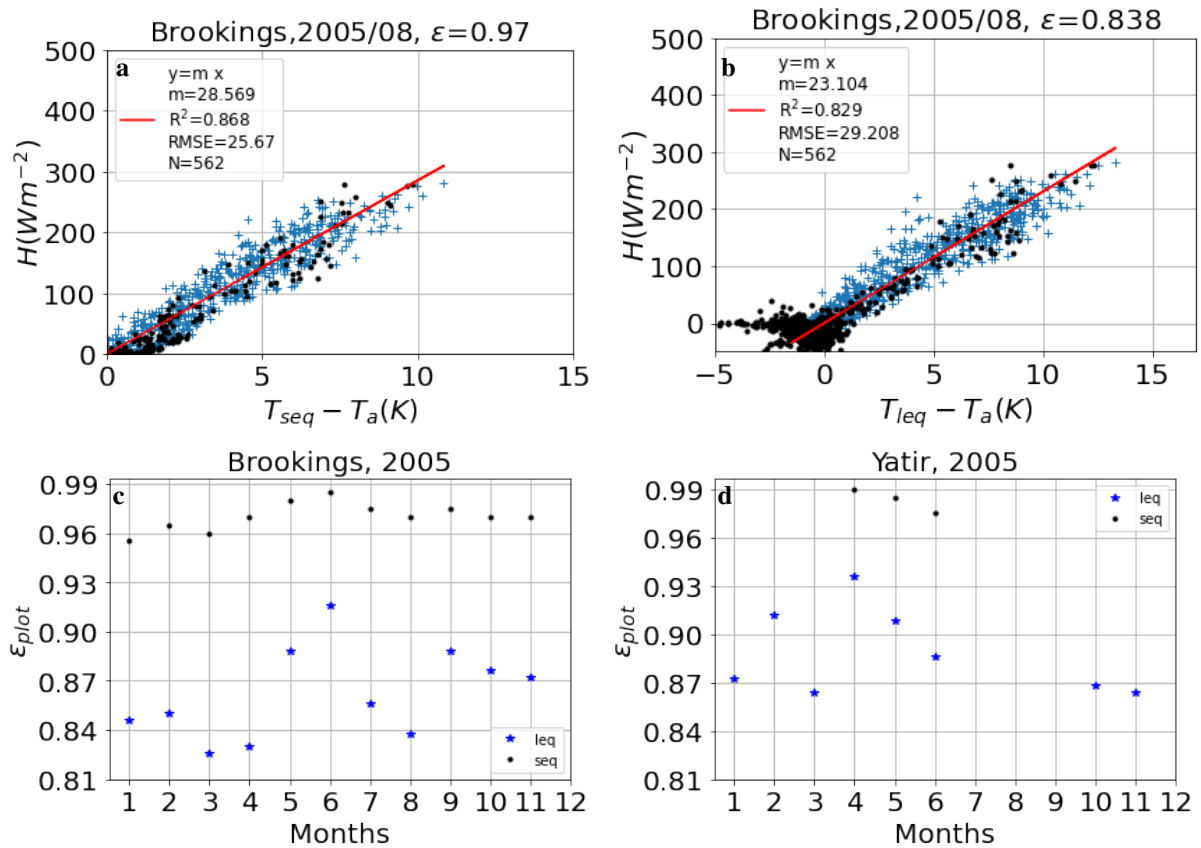

Figure 1. Reproduction of analysis presented in Figs. 2 (a) and 3 C and Q in Holmes et al. (2009)[18]. **(a)** Sensible heat (H) vs. $\Delta T = T_{seq} - T_a$ based on the short equation (T_{seq}, Eq. 12); (b) H vs. ΔT based on the complete equation (T_{leq}, Eq. 7). Both show data for August 2005 at Brookings. Blue crosses mark data points satisfying the filtering criteria while black dots mark points not considered in the analysis. N is the number of blue crosses used for regression (red line), m is the slope of regression, RMSE is the root mean square error and R^2 is the coefficient of determination. The fitted ε value is reported in the title. **(c)** Optimised ε values at Brookings obtained for the months where $R^2 > 0.5$ using the short equation (Eq. 11, black dots) and complete equation (Eq. 6, blue stars). **(d)** Same as (c), but for Yatir Forest. See Table 2 for site descriptions.

1.2 Landscape scale vs plot-scale estimates of ε and LST

At each site, LST was estimated using both the short equation (T_{seq}, Eq. 12) and the long equation (T_{leq}, Eq. 7). In the first step, tower-based longwave measurement and landscape-scale broadband ε from MODIS (ε_{MODIS}, Eq. 13) was used. The yearly daytime surface to air temperature difference for each study site is estimated is shown in Fig. 2. At all sites, Eq. 12 resulted in higher day-time plot-scale T_s estimates as compared to Eq. 7, when using ε_{MODIS}, with the medians of surface-air temperature differences (ΔT) differing by 0.8 to 1.5 K (Fig. 2). The difference in ΔT using two equation is highest at the water limited sites e.g AS, YA. Note that for two sites (LF and HS), the median values of daytime ΔT are negative.
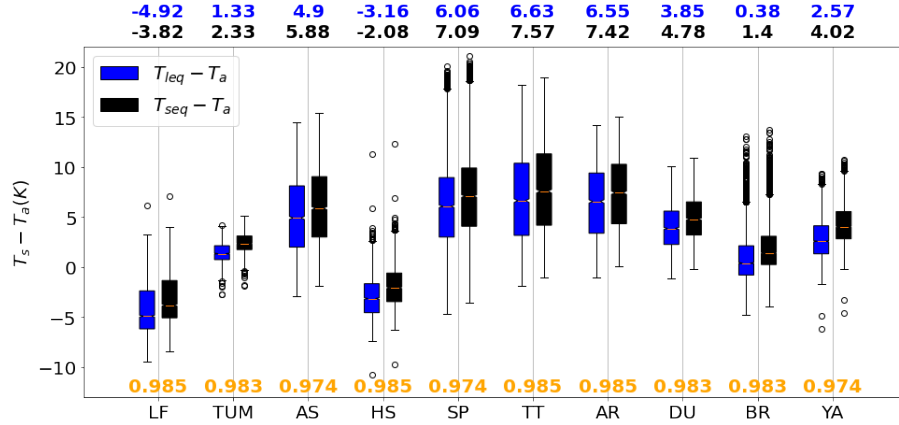

Figure 2. Yearly distributions of half-hourly surface to air temperature differences ($\Delta T = T_s - T_a$) for a representative year at each site. LST are inverted using short and long equation (Eq. 12), Eq. 7) with landscape-scale emissivity (ε_{MODIS}). The median values of ΔT are shown at top of the plot and the emissivities used for the T_s retrieval are shown at the bottom in orange. See Table 2 for site abbreviations.

Comparison of estimated plot-scale LST using ε_{MODIS} at satellite overpass time with landscape-scale LST (T_{MODIS}) revealed strong correlations between plot-scale and landscape-scale LST estimates as shown in Fig. 3a, b. Use of plot-scale ε_{plot} for plot-scale LST estimation (T_{seq} and T_{leq}) resulted in substantial reduction of the bias as shown in Fig. 3c, d. This trend in bias reduction was similar to other sites (Table **SI2** for details). The minimum bias is found at the Tumbarumba a closed canopy (eucalyptus forest) and highest bias was obtained at Litchfield and Howards Springs an sparse canopy (woodland savanna). However, for some sites, weak correlation between satellite-derived and local LST estimates were also evident (at DU, R^2 was reduced from 0.8 to 0.4, see Table **SI2**). Also, using plot-scale ε for LST estimation resulted in positive $T_s - T_a$ at LF and HS as shown in **SI3**.

1.3 Plot-scale ε estimation considering footprint mismatching of measurement devices

In order to account for the discrepancy in plot-scale ε estimation due to footprint mismatch of measuring devices H vs. ΔT relationship was allowed to accept an intercept as shown in Fig. 4. The plot-scale ε using long equation with an intercept results into the conventional (realistic) range of emissivity in comparision to the one with no intercept at study sites as shown in Table (1). The intercept value for Brookings, a grassland is 12% of maximum sensible heat flux (H_{max}) and for a mulga shrubs like AS is 20% of H_{max}. The intercept value for HS is 70% of H_{max} and for Tum is 7% of H_{max}. The intercept value is lowest for a forest site (closed canopy) and highest for a sparse canopy (HS, mix of tree, grass and bare soil). The comparison of resulting plot-scale LST with landscape-scale LST Table shows an increase in bias with respect to the LST obtained using ε without an intercept as shown in Table. (1).

1.4 Uncertainty in plot-scale ε and LST due to measurement error

Each of the observed input variables used for the estimation of plot-scale ε and LST has a certain level of measurement uncertainty associated with it. To quantify the propagation of these uncertainties using the two equations(Eq. 12, Eq. 7) without and with an intercept in H versus Δ T relationship, we plotted the ranges of results obtained by random perturbations of each input variable within its own measurement (uncertainty) bounds. Here we present results for Alice Springs, which showed the highest correlation between plot-scale and landscape-scale estimations of LST (Table **SI2**). The uncertainty in plot-scale ε estimated using Eq. 7 without allowing an intercept for $H(\Delta T)$ ranged between 0.68 and 0.98 whereas ε estimated with allowing an intercept $H(\Delta T + c)$ revealed very constrained values as shown by the green boxes.The short equation (Eq.12) also resulted in constrained values between 0.94 and 0.99 (Fig. 5a). The uncertainty in hourly $T_s - T_a$ is estimated using uncertainty
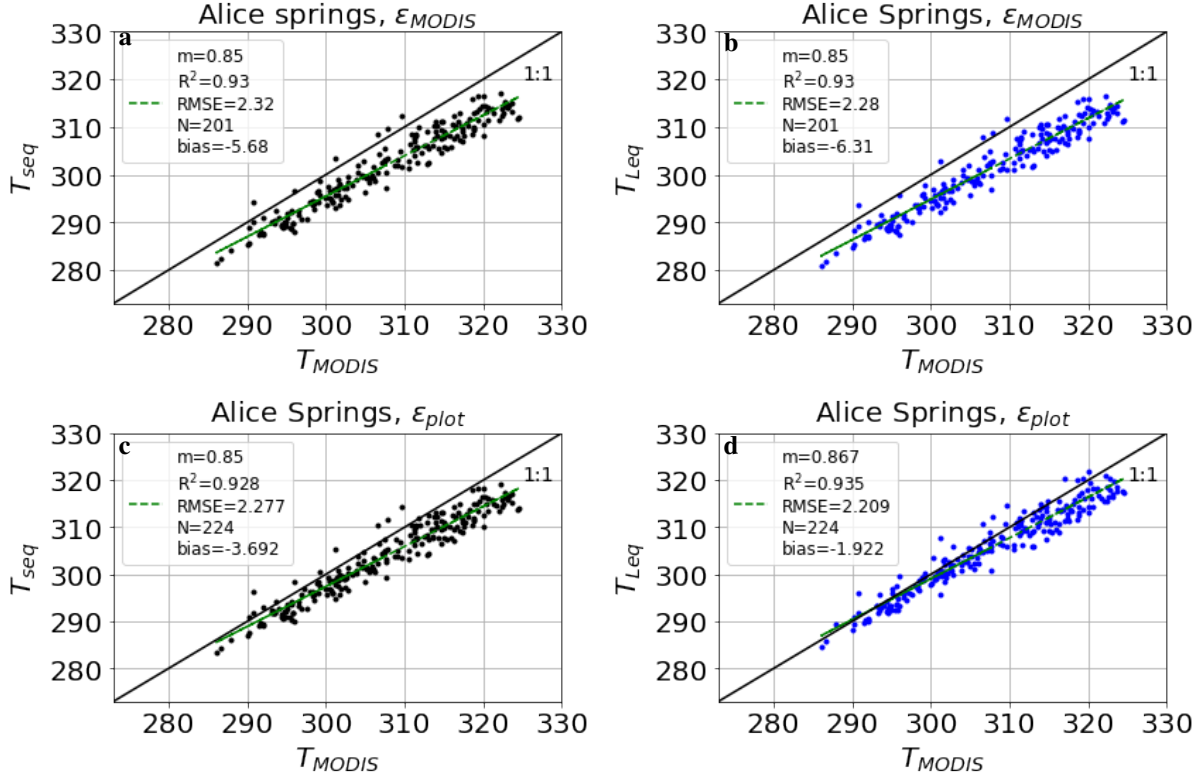
Figure 3. Landscape-scale LST (T_{MODIS} derived from MOD11A1) vs. plot-scale LST at Alice Springs for 2016-2018. **(a)** T_{seq} based on short equation (Eq. 12) and satellite-derived (MODIS) landscape-scale broadband emissivity; **(b)** Same as (a), but T_{leq} based on complete equation (Eq. 7); **(c)** T_{seq} based on short equation (Eq. 12) and monthly plot-scale emissivity; **(d)** Same as (c), but T_{leq} based on complete equation (Eq. 7). Bias is mean $T_{seq} - T_{MODIS}$, N is the number of daily overpasses of MODIS between 2016 and 2018, c is the intercept, m the slope, RMSE is the root mean square error and R^2 is coefficient of determination. At each site, LST was estimated using both the short equation (T_{seq}, Eq. 12) and the long equation (T_{leq}, Eq. 7). In a first step, we used satellite-derived landscape-scale broadband emissivity from MODIS (ε_{MODIS}, Eq. 13) for estimating plot-scale LST from tower-based longwave measurements, and compared these with landscape-scale LST extracted from daily MODIS LST images (T_{MODIS})

in plot-scale ε was quite similar for both complete and simplified equation (blue and black boxes in Fig. **??**). The uncertainty in $T_s - T_a$ was higher when landscape-scale ε was used (Fig. 5b, c).

2 Discussion

Our analysis revealed the deficiency in commonly used short equation for estimating plot-scale LST and ε. The use of complete equation for plot-scale ε estimation results into lower values for sparse canopy. In order to obtain realistic ε for sparse canopy conceding footprint mismatch between radiometric and aerodynamic footprint becomes important.

Depending on the equation (Eq. 7 or Eq. 12) used to estimate LST, small approximation (error) in ε can lead to large error in LST. The sensitivity of the long equation (Eq. 7) to ε is driven by the contrast between R_{lup} and R_{ldwn} whereas for short equation (Eq. 12) it is only driven by observed R_{lup}. For instance an error of 0.01 in ε at water limited sites like AS can cause an error of $0.17K$ using Eq. 7 and $0.79K$ using Eq. 12 respectively. This shows a clear advantage of Eq. 7 for plot-scale LST estimation since most of the time ε is used as an approximate value. Also plot-scale ε estimation using long equation (Eq. 7) results in $H(\Delta T)$ relationship for more months (Fig. 1d). However, ε estimates using Eq. (7) are lower than Eq. (12) and in particular for sites like HS and LF the ε was unrealistic Table.**SI** 4 in comparison to the previously reported ε values for a soil-vegetation system[34,35]. The lower ε value using correct equation (Eq. 7, Fig. 1b) Table 1 suggests problem due to combining measurements coming from instruments characterized by different footprints[22]. The mismatch of source areas (footprint) of radiometric and aerodynamic flux measurements becomes important if the surface underlying the instruments is heterogeneous (e.g. AS,TT, YA, AS, HS, LF). The mismatch in footprint can further results into $H \neq 0$ at $\Delta T = 0$. This problem was not detected for Holmes et.al[36] as short equation (Eq. 12) was used and due to its high sensitivity to ε (**SI Fig. 10**
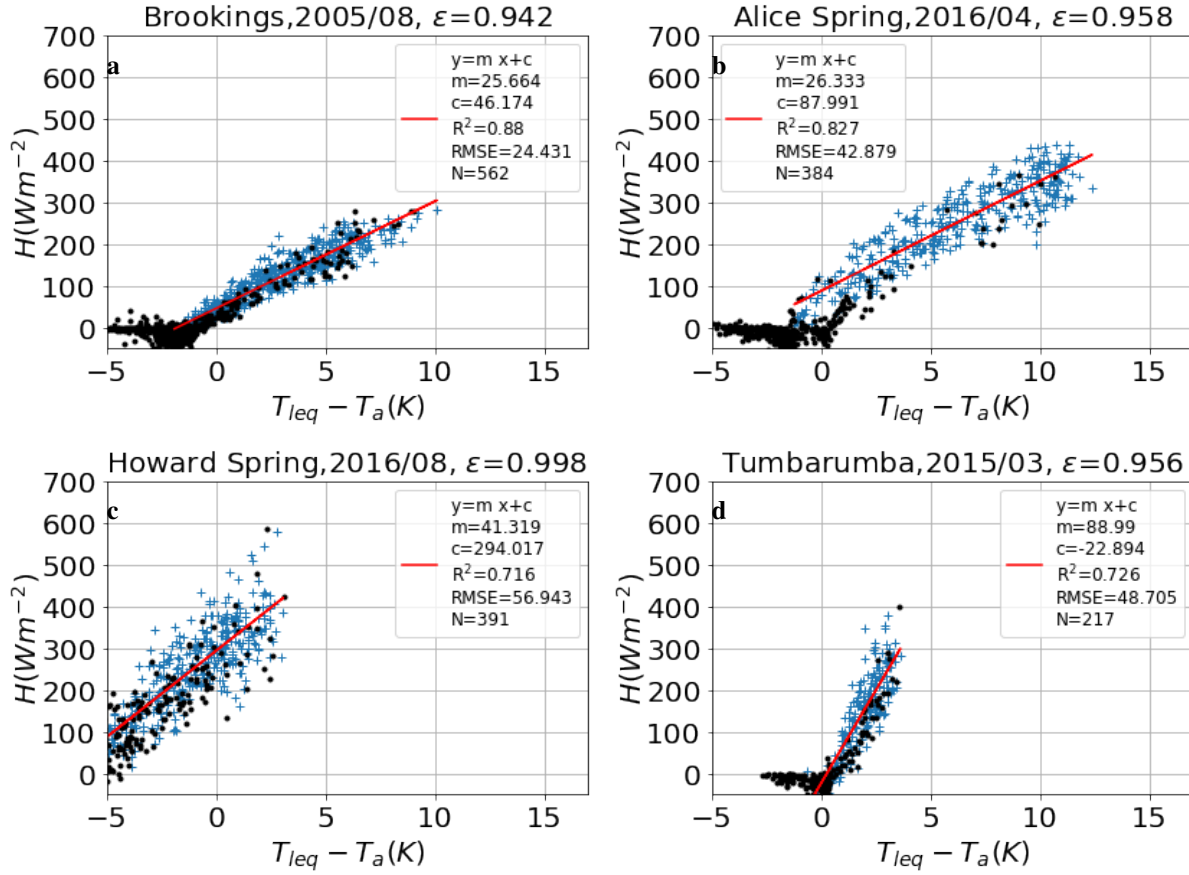
Figure 4. Using robust linear regression $H = m(T_s - T_a) + c$. The ε is estimated by minimising RMSE. The title of the plot shows site, year, month and the ε. The legend correspond to Fig. 1 and c is interpreted as the H from the aerodynamic footprint which is not seen by the radiometer.

Sites	Landscape-scale ε			Plot-scale ε $H = m * (\Delta T)$			Plot-scale ε $H = m * (\Delta T) + c$			
	ε_{land}	R^2	bias	ε_{plot}	R^2	bias	ε_{plot}	R^2	bias (K)	c
SP	0.974	0.81	-4.61	0.85	0.82	-1.91	0.92	0.774	-2.563	18.12
AS	0.974	0.93	-6.24	0.82	0.93	-1.92	0.993	0.915	-4.884	72.46
TT	0.974	0.57	-8.30	0.80	0.52	-4.02	0.939	0.521	-7.466	58.70
HS	0.985	0.16	-9.90	0.6	0.22	-2.47	0.949	0.18	-10.45	237.29
LF	0.985	0.41	-11.0	0.6	0.41	-2.57	0.968	0.378	-11.47	258
AR	0.985	0.27	-3.51	0.960	0.252	-2.98	0.996	0.27	-3.567	14.72
DU	0.985	0.81	4.61	0.985	0.425	-3.926	0.994	0.405	-4.603	-8.11
TUM	0.983	0.84	-2.10	0.97	0.89	-1.93	0.955	0.85	-1.696	-24.24
BR	0.983	0.937	-0.195	0.82	0.895	2.72	0.919	0.906	1.662	17.72
YA	0.974	0.855	-3.45	0.93	0.793	-0.582	0.873	0.826	0.073	-22.95

Table 1. Comparison of daytime landscape-scale LST (T_{MODIS}) with plot-scale LST (T_s) estimated at TERRA time of pass using long equation. The emissivity used to retrieve plot scale LST is derived using relationship without intercept $H(\Delta T)$ and with intercept ($H((\Delta T) + c(H)$)at study sites are reported. The reported plot-scale emissivity are median values and landscape emissivity are MODIS based. Bias is defined as mean of $T_s - T_{MODIS}$, R^2 is coeffecient of determination between plot-scale LST in comparison to landscape-scale LST. The site acronyms can be found in Table 2.

a) even with small reduction in ε the offset in $H(\Delta T)$ was corrected (Fig. 1a). Whereas due to lower sensitivity of Eq. 7 to ε (SI Fig. 10 a) larger reduction is required to get rid of intercept resulting into lower ε as shown in Fig. 1b. We proposed an improvement to the method by allowing an intercept in $H(\Delta T)$ regression (robust regression). Considering aerodynamic
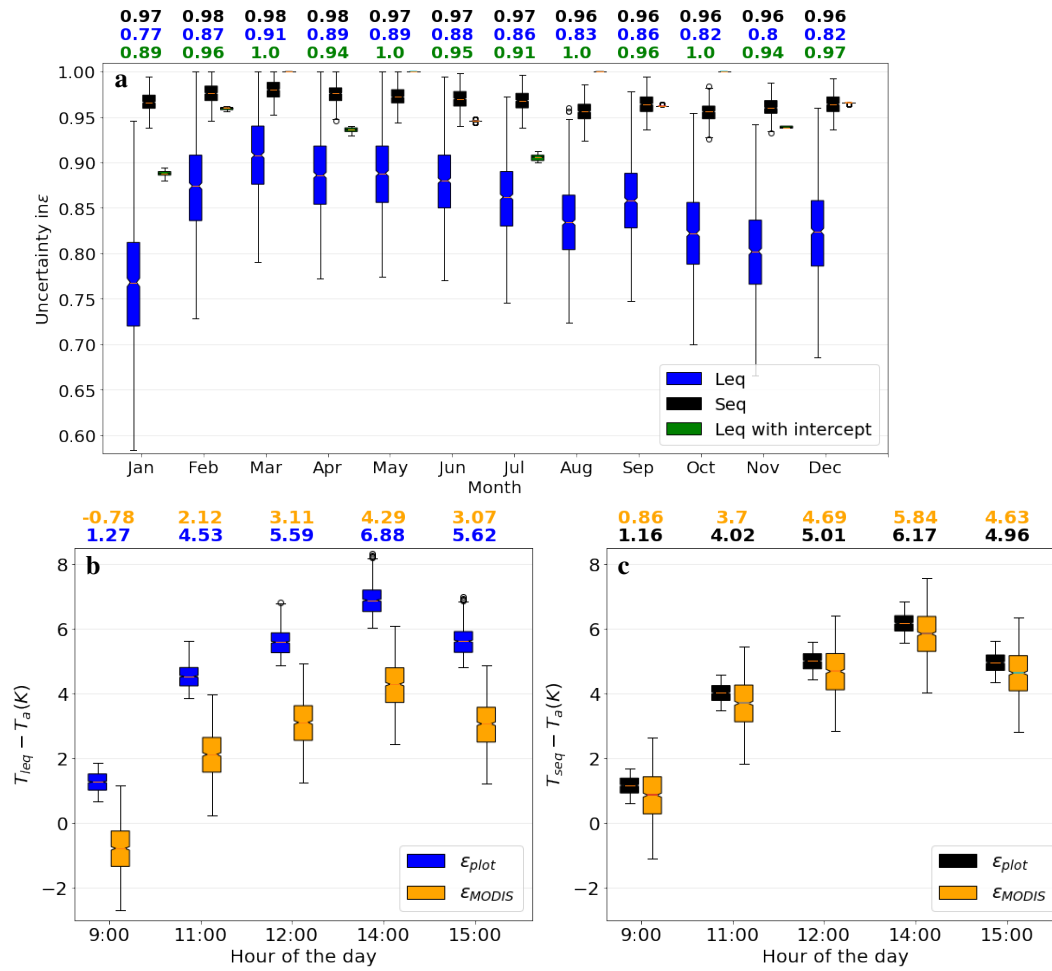
Figure 5. Uncertainty in monthly emissivity for 2017 and hourly $T_s - T_a$ for 15 August 2017. **(a)** Uncertainty in monthly optimised emissivity due to uncertainty in H, R_{lup}, R_{ldw}, T_a at using Eq. (6) and Eq. (11) shown in Blue and black for 2017 at AS. **(b)** Hourly daytime uncertainty in $T_s - T_a$ due to perturbed fluxes and optimum ε using Eq. (6) in blue. optimum ε using Eq. (6) in green and perturbed fluxes with MODIS based ε in orange(Fig. (2). **(c)** Hourly daytime uncertainty in $T_s - T_a$ due to perturbed fluxes and optimum ε using Eq. (11) in black and perturbed fluxes with MODIS ε in orange. Unperturbed optimum ε values and $T_s - T_a$ values correspond to the median of perturbed values

footprint to be greater than radiometric footprint[22] the offset was interpreted as the H from aerodynamic footprint which is not seen by the radiometer. And it resulted into realistic ε (Fig 4a, b, c, d) but intercept was very high for sites like HS and LF Table. 1. Looking closely at $H(\Delta T)$ plots for HS and LF and placing high value of intercept and lower daytime $T_s - T_a$ into perspective we could hypothesize an underestimation of R_{lup}. Testing the hypothesis for HS we found that adding roughly 40 $Wm-2$ (approx 8% of observed R_{lup}) in observed R_{lup} led to significant reduction in the intercept from $294Wm-2$ (Fig. 4 c) to $17Wm-2$ with positive $T_s - T_a$ as shown in Fig. 6 a). The other linear regression parameter (m, R^2, RMSE) donot remained constant for Fig. 6a and Fig. 6c. Reminding ourselves the hemispherical view of the radiometers looking down at the canopy makes it a possible scenario a sparse canopy like HS and LF[22,37]. And radiometer will see more tree crowns and less soil which can lead to appoximately 5-10% underestimation of R_{lup} (**SI 6**, Fig. 12). As shown in Fig. 4 the offset was proportional to the maximum observed H for each and an illustration plot for 36 months for AS is shown in Fig. 4 (**SI 7** Fig. 13). The ratio between H_{max} and intercept (c) varies between 0% to 30% for AS. The seasonality of ratio can be attributed to the change in solar angle and the dominant wind direction. Surface heterogeneity has also been recognized as one of the potential causes of the lack of energy balance closure observed at most ECS[38,39] at diurnal scales which further leads to underestimation of turbulent fluxes (H, LE). Therefore as a prerequisite the observed turbulent fluxes are corrected using an energy balance closure scheme[40] and used. However, in our analysis the use of energy balance closure scheme (based on Bowen ratio) led to much lower value of plot-scale ε using Holmes approach[18,33]. Similar studies on plot-scale ε estimation have used the observed fluxes without correction[20,36,41,42]. The use of energy balance closure scheme for the for plot-scale ε estimation led to an increase in positive intercept (sparse canopy, Fig. 4). We also looked into the intercept of $H(\Delta T)$ at minimum range of energy imbalance also

results into high intercept as shown in Fig 6 b. Our analysis shows that although surface heterogenity is one of the common reason for the intercept in $H(\Delta T)$ and lack of energy balance closure but the relation between the two is non conclusive.
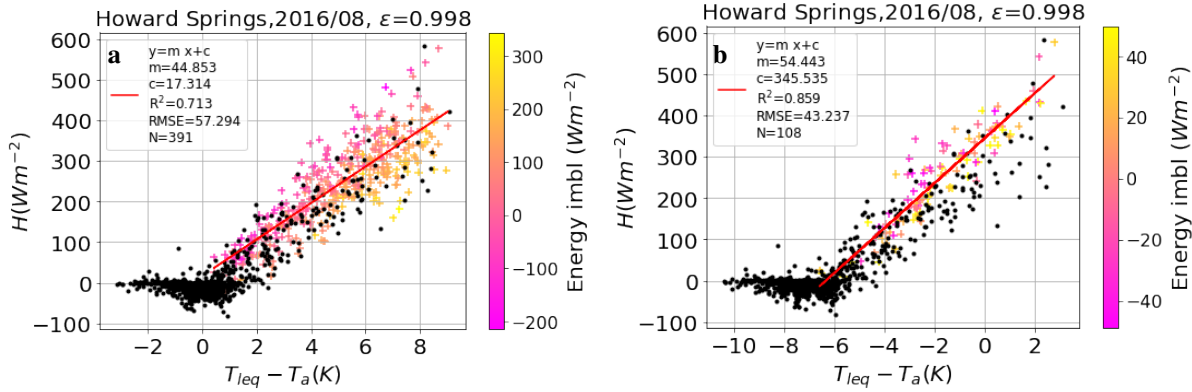

Figure 6. $H vs \Delta T$ using reboust linear regression, the crosses (see Fig. 4 c) are color coded according to the energy imbalance $(R_n - H - LE - G)$ (a) By adding 40 (Wm^{-2}) to measured R_{lup} led to significant reduction in the intercept from $294 Wm-2$ (Fig. 4 c) to $17 Wm-2$ with increase in $T_s - T_a$. (b) Choosing data points where energy imbalanceis between -50 to 50 (Wm^{-2}) intercept is increased from $294 Wm-2$ (Fig. 4 c) to $345 Wm-2$. The legends crosspond to Fig. 4

Comparison of plot-scale LST with MODIS LST resulted into very high bias for sparse canopy which is in agreement with previous studies where the bias for sparse canopy was high upto $12K$[43]. Plot-scale LST estimate using plot-scale ε decreased the bias in comparsion to MODIS LST as shown in Table 4. The use of plot-scale ε also reduces the uncertainty in diurnal LST in comparsion to landscape-scale ε (Fig. 5 b,c). However LST estimated using plot-scale ε considering foot print mismatch $(H = m * \Delta T + c)$ resulted into increase in bias for most of the study site as shown in Table. 1. The increase in bias could be attributed to implicit consideration of spatial heterogenity (by accepting intercept) at plot-scale whereas, MODIS LST (landscape-scale) are integrated pixel information considering radiating signal from a homogeneous surface.

The fluxes observed at a soil-vegetation system is representative of the composite signal from both soil and vegetation which typically have a different range of surface temperatures and emissivities[11]. The ε of soil strongly depends on soil moisture content[44]. Whereas the emissivity of a canopy depends on its structure attributes and leaf area index, the latter of which varies strongly at the seasonal scale[45]. For example, laboratory-measured directional ε for various canopy elements (bark, leaf and its arrangement, stem wood) ranged between 0.9 to 1[46]. Laboratory measurements of thermal infrared reflectance spectra suggests that the ε variation from structural unknowns, such as leaf orientation, is more significant than the differences in leaf component emissivity among plant species[35]. Consequently it is clear that the ε of a surface is a function of many factors and detailed study of all these factors is out of scope of the present study. Thus, derivation of landscape-scale broadband ε_{land} from narrowband spectral emissivity is considered as a first-order approximation for capturing the integrated effects of land cover from MODIS spectral bands[11]. However, due to general lack of emissivity information for natural ecosystem at ECS, remotely sensed emissivity serves as plausible estimates and are valuable input for plot-scale LST estimation. Plot-scale ε by fitting observed H and estimated ΔT without an intercept results into a lower value and is statistically questionable[47]. Since fluxes observed at ECS contain composite (soil and vegetation) signal and is represented as area weighted average plot-scale ε by allowing an intercept $H(\Delta T)$is a statistically correct and results into realistic ε for sparse canopy. Estimation of an intrinsic property like surface emissivity using time varying fluxes can be questioned however considering the spatial and temporal limitation of satellite derived data the plot-scale ε estimation is a good alternative.

Our analysis shows that under no condition for grey bodies the use of simplified equation and complete equation can lead to equal values of ε and LST and thus thewe should stop using simplified equation. Considering widely spread use of ECS recorded fluxes and MODIS LST for model calibration and validation,the use plot-scale ε can be advantageous as it reduces the bias between plot-scale and MODIS LST in comparison to MODIS ε. Plot-scale ε reduces the uncertainty in diurnal LST due to measurement errors.The implication of our study can be particularly interesting for the research community interested to understand diurnal and seasonal feedback in soil-vegetation system with the flux, emissivity and LST estimated at a consistent scale. This work can also be used to calibrate and validate the LSM at ecosystem scale.

3 Methods

3.0.1 Research data

Tower data ECS collect micro-meteorological measurements above the surface (vegetation canopy) using towers (flux tower), following common measurement protocols[12]. The towers are commonly equipped with an instrument made up of pyrgeometers

or radiometers to measure up-welling and down-welling shortwave and longwave radiation, which is further used to calculate net radiation (Eq. 3). Besides radiative fluxes, measurement at EC towers also include sensible and latent heat fluxes, net carbon dioxide exchange and a range of meteorological variables, such as air temperature, humidity and wind speed. T_a is the air temperature measured using eddy ECS mounted above the canopy. Each flux measurement is accompanied by a flagging system and follows the agreement with second CarboEurope-IP QA/QC workshop[48]. Flag 0 is designated as high data quality, and have been used in our current work. For the analysis 10 sites were selected to represent a variety of land cover types and climates (Table 2). 8 sites belong to the North Australian Tropical Transect (NATT) and 2 sites (Yatir Forest, Brookings) are chosen to replicate result from Holmes et.al[36]. Eddy covariance Level 3 data is obtained from http://data.ozflux.org.au/portal/pub/listPubCollections.jspx for Australian sites. The data for Brookings in obtained from ameriflux and for Yatir Forest the data was obtained using personal communication to Prof Dan Yakir's lab group as the data used in Holmes work was from 2005[18] and the current available data was an updated version of the fluxnet data.

MODIS data Landscape- scale emissivity and LST data (MODIS product MOD11A1) was downloaded downloaded from NASA earth data . It is a level 3 daily LST product gridded in the sinusoidal projection at a spatial resolution of 0.928 *km* by 0.928 *km*. A tile contains 1200 x 1200 grids in 1200 rows and 1200 columns[49]. The daily LST pixel values in each granules is retrieved by the generalized split-window algorithm under clear-sky conditions and LST values are averaged by overlapping pixels in each grid with overlapping areas as weight. The downloaded data are in Hierarchical Data Format (hdf) which were converted into tagged image file format (tiff) using a python package called PyModis[50]. From tiff the files are converted into csv format. The details of data extraction and conversion can be found at $https://renkulab.io/projects/gitanjali.thakur/modis_lst_fpar/$. The dataset columns used to compare plot-scale LST and emissivity are : day time daily LST, local view time, night view time, channel 31, 32 spectral ε respectively.

Site-specific approach This approach was initially proposed by Holmes[36] to estimate plot-scale ε using short equation with H, R_{lup}, T_a. In present work we have used both long equation (Eq. 7) and short equation (Eq. 7) to estimate ε The prime variable used in the study are $H, R_{lup}, R_{ldwn}, T_a$ and the ancillary variable are R_n and wind speed (Ws) are used to filter the data for analysis. The filtering condition were $R_n > 25 Wm^-2$) and wind speed ($Ws > 2ms^-1$)[18]. Plot scale emissivity is derived by segregating each month data satisfying the filtering criteria. For estimating T_s from longwave measurement(R_{lup}, R_{ldwn}) a predefined range of ε is chosen starting from 0.998 and is reduced at a step size of 0.002. For each month data $H(T_s - T_a)$ linear regression is performed using scipy $https://docs.scipy.org/doc/scipy-0.14.0/reference/generated/scipy.stats.linregress.html$. The R^2 is checked and months where $R^2 > 0.5$ (i.e substantial part of variance in H is explained by $T_s - T_a$) is chosen for ε estimation. To obtain *epsilon* regression line of $H, \Delta T$ is forced through origin (at $T_s - T_a = 0$ $H = 0$) by minimising the RMSE. An illustration plot for RMSE and ε is shown in **SI5**. The ε_{plot} is obtained for each month using both long Eq.(7) and short equation Eq.(12) and termed as ε_{seq} and ε_{leq} as shown in Fig. 7b. In the next step instead of forcing the $H vs \Delta T$ plot through origin robust linear regression is used, which allowed an offset in monthly $H(\Delta T)$ plots. The plot-scale ε was obtained by minimising RMSE as explained before. Plot-scale LST estimated using plot-scale ε was compared to landscape-scale MODIS LST. Monthly tower based longwave measurement at study sites corresponding to TERRA daily time of pass was obtained using linear interpolation. TERRA (satellite) overpasses at local solar time between 10:30 am to 12 pm in ascending mode[13]. Plot-scale LST ((T_{leq} and T_{seq}) was obtained using interpolated day time longwave measurement and crossponding month plot-scale ε using Eq. (7), Eq. (12) . Plot-scale daily LST is compared to MODIS LST in terms of mean, bias, RMSE and R^2 using a robust linear regression model(scipy stat model) as shown in Fig. 7a. The goodness of fit between plot-scale and landscape-scale LST was determined by looking at (R^2) as shown in Fig. 7b. The bias is estimated as mean of deviation between daily MODIS LST and ground based T_s ($T_{leq,seq} - T_{MODIS}$). See SI table for data sources and acronyms in **SI1**

General Approach In this approach we estimate Landscape-scale ε (Broadband) is estimated using MODIS spectral ε as shown[51]

$$\varepsilon_{MODIS} = 0.4587\varepsilon_{31} + 0.5414\varepsilon_{32} \tag{13}$$

Tower based longwave measurement (R_{lup}, R_{ldwn}) passing the filtering criteria (as mentioned in site- specific approach) along with MODIS based ε was used to invert LST using Eq. (7) and Eq. (12). Plot-scale LST estimated using MODIS based ε was compared to landscape-scale MODIS LST using a robust linear regression as done in site specific approach as shown in Fig. (7a).

Uncertainty estimation The uncertainty in plot-scale ε due to error is observed fluxes is estimated. In first step, the error bounds of each input variables (H, R_{lup}, R_{ldw}, T_a) is assumed. The error bounds for $R_{lup} R_{ldwn}$ are -5 to 5 W m^{-2}[28], for H is -20 to 20 W m^{-2} and for T_a it is -1 to 1 K[40]. Uniformly distributed samples within error bounds are generated using saltelli sampling scheme[52] using python based package name SALIB. Each error samples are added to the monthly segregated measured fluxes. The plot-scale ε is estimated for the fluxes with added uncertainty (error sample) as explained in site specific approach. The obtained range of plot-scale ε is reported as uncertainity in emissivity . The plot-scale ε uncertainty with uncertainty in R_{lup}, R_{ldw} is used to calculate the uncertainty in hourly LST using short equation Eq. 12 and long equation Eq.7

Table 2. Description of study sites

Study site	latitute, longitude	Landcover	Time-period	longwave sensors	Sensor installation height (m)
Sturt Plains (SP)	-17.1507, 133.3502	Mitchell Grass	2016-2019	CG-2	4.8
Alice Springs (AS)	-22.2828, 133.2493	Mulga woodland, hummock grassland, river red gum forest	2016-2018	CNR1	12.2
Ti Tree East (TT)	-22.2870, 133.6400	Grassy mulga woodland, Corymbia/Triodia savanna	2016-2018	CNR1	9.9
Howard Springs (HS)	-12.4943, 131.1523	Open woodland savanna	2016-2018	CM-7B, CG-2	23
Litchfield (LF)	-13.1790, 130.7945	Tropical savanna	2016-2018	CNR4	31
Adelaide River (AR)	-13.0769, 131.1178	Savanna dominated by Eucalyptus tectifica and Planchonia careya	2006-2009	CNR1	15
Daly Uncleared (DU)	-14.1592, 131.3881	Woodland savanna	2016-2018	NRlite	21
Tumbarumba (TUM)	-35.6566, 148.1517	Wet sclerophyll	2015-2018	CM3 and CG3	70
Brookings (BR)	44.352, 96.840	Cropland	2005	pyrgeometers[13]	NA
Yatir Forest (YF)	35.052, 31.345	Evergreen needleleaf forest	2005	pyrgeometers[13]	NA

as shown in Fig. 5b,c. .

4 Acknowledgements

References

1. Still, C. J. *et al.* Imaging canopy temperature: shedding (thermal) light on ecosystem processes. *New Phytol.* **230**, 1746–1753 (2021).

2. Mallick, K. *et al.* Reintroducing radiometric surface temperature into the p enman-m onteith formulation. *Water Resour. Res.* **51**, 6214–6243 (2015).

3. Zheng, W. *et al.* Improvement of daytime land surface skin temperature over arid regions in the ncep gfs model and its impact on satellite data assimilation. *J. Geophys. Res. Atmospheres* **117** (2012).
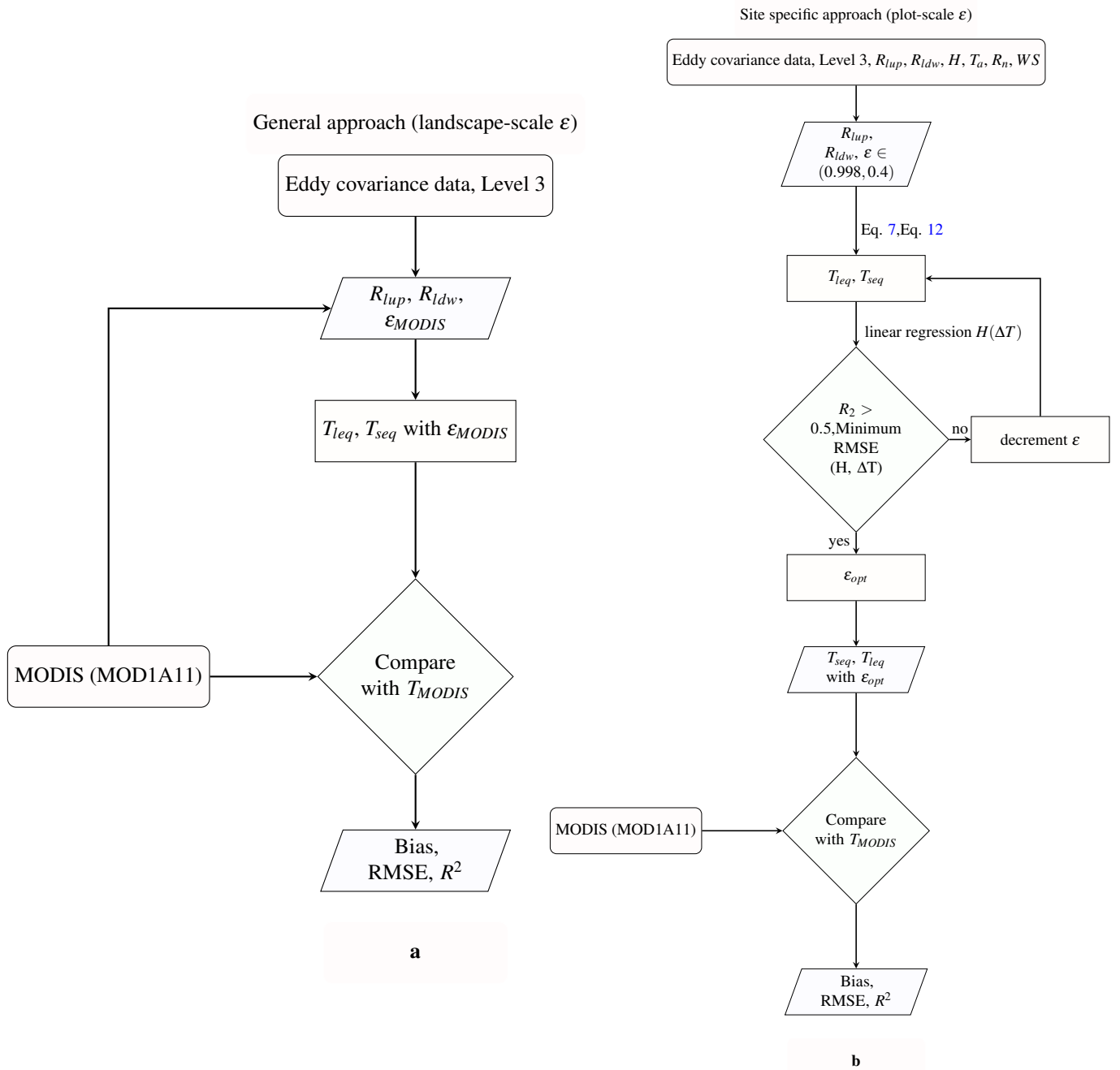
Figure 7. Schematic representation of steps followed for plot scale LST retreival using eddy covariance measurement(a) Landscape emissivity and longwave measurement and compared to Landscape-scale LST(T_{MODIS}).(b) Plot-scale emissivity estimation using observed H, R_{ldwn}, R_{lup} and plot-scale LST is estimated using plot-scale ε is compared to landscape-scale emissivity. The R^2, RMSE, Bias are mentioned in Fig. (3)

4. Koch, J., Siemann, A., Stisen, S. & Sheffield, J. Spatial validation of large-scale land surface models against monthly land surface temperature patterns using innovative performance metrics. *J. Geophys. Res. Atmospheres* **121**, 5430–5452 (2016).

5. Kustas, W. P., Anderson, M. C., Norman, J. M. & Li, F. Utility of radiometric–aerodynamic temperature relations for heat flux estimation. *Boundary-Layer Meteorol.* **122**, 167–187 (2007).

6. Norman, J. M. & Becker, F. Terminology in thermal infrared remote sensing of natural surfaces. *Agric. For. Meteorol.* **77**, 153–166 (1995).

7. Wang, K. Estimation of surface long wave radiation and broadband emissivity using Moderate Resolution Imaging Spectroradiometer (MODIS) land surface temperature/emissivity products. *J. Geophys. Res.* **110**, D11109, DOI: 10.1029/2004JD005566 (2005).

8. Hulley, G. C., Hughes, C. G. & Hook, S. J. Quantifying uncertainties in land surface temperature and emissivity retrievals from ASTER and MODIS thermal infrared data. *J. Geophys. Res. Atmospheres* **117**, DOI: 10.1029/2012JD018506 (2012).

9. Jin, M. & Liang, S. An improved land surface emissivity parameter for land surface models using global remote sensing observations. *J. Clim.* **19**, 2867–2881 (2006).

10. Wang, K. & Liang, S. Evaluation of ASTER and MODIS land surface temperature and emissivity products using long-term surface longwave radiation observations at SURFRAD sites. *Remote. Sens. Environ.* **113**, 1556–1565, DOI: 10.1016/j.rse.2009.03.009 (2009).

11. Jin, M. & Liang, S. An Improved Land Surface Emissivity Parameter for Land Surface Models Using Global Remote Sensing Observations. *J. Clim.* **19**, 2867–2881, DOI: 10.1175/JCLI3720.1 (2006).

12. Baldocchi, D. *et al.* Fluxnet: A new tool to study the temporal and spatial variability of ecosystem-scale carbon dioxide, water vapor, and energy flux densities. *Bull. Am. Meteorol. Soc.* **82**, 2415–2434 (2001).

13. Guillevic, P. *et al.* Land surface temperature product validation best practice protocol. version 1.0. *Best Pract. for Satell. Land Prod. Valid.* 60 (2017).

14. Wang, K. & Dickinson, R. E. Global atmospheric downward longwave radiation at the surface from ground-based observations, satellite retrievals, and reanalyses: DOWNWARD LONGWAVE RADIATION. *Rev. Geophys.* **51**, 150–185, DOI: 10.1002/rog.20009 (2013).

15. Sun, J. & Mahrt, L. Relationship of surface heat flux to microscale temperature variations: Application to boreas. *Boundary-Layer Meteorol.* **76**, 291–301 (1995).

16. Jacob, D. *et al.* A comprehensive model inter-comparison study investigating the water budget during the baltex-pidcap period. *Meteorol. Atmospheric Phys.* **77**, 19–43 (2001).

17. Lhomme, J.-P., Katerji, N., Perrier, A. & Bertolini, J.-M. Radiative surface temperature and convective flux calculation over crop canopies. *Boundary-Layer Meteorol.* **43**, 383–392, DOI: 10.1007/BF00121714 (1988).

18. Holmes, T. R. H., Jeu, R. A. M. D., Owe, M. & Dolman, A. J. Land surface temperature from Ka band (37 GHz) passive microwave observations. *J. Geophys. Res. Atmospheres* **114**, DOI: 10.1029/2008JD010257 (2009).

19. Holmes, T. R. H., Hain, C. R., Anderson, M. C. & Crow, W. T. Cloud tolerance of remote-sensing technologies to measure land surfacetemperature. *Hydrol. Earth Syst. Sci.* **20**, 3263–3275, DOI: 10.5194/hess-20-3263-2016 (2016).

20. Maes, W. H., Gentine, P., Verhoest, N. E. & Miralles, D. G. Potential evaporation at eddy-covariance sites across the globe. *Hydrol. Earth Syst. Sci.* **23**, 925–948 (2019).

21. Chu, H. *et al.* Representativeness of eddy-covariance flux footprints for areas surrounding ameriflux sites. *Agric. For. Meteorol.* **301**, 108350 (2021).

22. Marcolla, B. & Cescatti, A. Geometry of the hemispherical radiometric footprint over plant canopies. *Theor. Appl. Climatol.* **134**, 981–990 (2018).

23. Morillas, L. *et al.* Using radiometric surface temperature for surface energy flux estimation in mediterranean drylands from a two-source perspective. *Remote. Sens. Environ.* **136**, 234–246 (2013).

24. Rannik, Ü., Peltola, O., Mammarella, I. *et al.* Random uncertainties of flux measurements by the eddy covariance technique. *Atmospheric Meas. Tech.* (2016).

25. Mauder, M., Foken, T. & Cuxart, J. Surface-energy-balance closure over land: a review. *Boundary-Layer Meteorol.* **177**, 395–426 (2020).

26. Vickers, D., Göckede, M. & Law, B. Uncertainty estimates for 1-h averaged turbulence fluxes of carbon dioxide, latent heat and sensible heat. *Tellus B: Chem. Phys. Meteorol.* **62**, 87–99 (2010).

27. Wang, K. & Liang, S. Evaluation of ASTER and MODIS land surface temperature and emissivity products using long-term surface longwave radiation observations at SURFRAD sites. *Remote. Sens. Environ.* **113**, 1556–1565, DOI: 10.1016/j.rse.2009.03.009 (2009).

28. Trenberth, K. E. & Fasullo, J. T. Tracking earth's energy: From el niño to global warming. *Surv. geophysics* **33**, 413–426 (2012).

29. Crago, R. D. & Qualls, R. J. Use of land surface temperature to estimate surface energy fluxes: Contributions of Wilfried Brutsaert and collaborators. *Water Resour. Res.* **50**, 3396–3408, DOI: 10.1002/2013WR015223 (2014).

30. Stephens, G. L. Review of atmospheric radiation: 1991–1994. *Rev. Geophys.* **33**, 785–794 (1995).

31. Crago, R. D. & Qualls, R. J. Use of land surface temperature to estimate surface energy fluxes: Contributions of Wilfried Brutsaert and collaborators. *Water Resour. Res.* **50**, 3396–3408, DOI: 10.1002/2013WR015223 (2014).

32. Rosolem, R., Gupta, H. V., Shuttleworth, W. J., Zeng, X. & De Gonçalves, L. G. G. A fully multiple-criteria implementation of the sobol' method for parameter sensitivity analysis. *J. Geophys. Res. Atmospheres* **117** (2012).

33. Holmes, T. R. H., Hain, C. R., Anderson, M. C. & Crow, W. T. Cloud tolerance of remote-sensing technologies to measure land surfacetemperature. *Hydrol. Earth Syst. Sci.* **20**, 3263–3275, DOI: 10.5194/hess-20-3263-2016 (2016).

34. Sugita, M. & Brutsaert, W. Optimal Measurement Strategy for Surface Temperature to Determine Sensible Heat Flux From Anisothermal Vegetation. *Water Resour. Res.* **32**, 2129–2134, DOI: 10.1029/96WR00993 (1996).

35. Snyder, W. C., Wan, Z., Zhang, Y. & Feng, Y.-Z. Classification-based emissivity for land surface temperature measurement from space. *Int. J. Remote. Sens.* **19**, 2753–2774 (1998).

36. Holmes, T. R. H., Jeu, R. A. M. D., Owe, M. & Dolman, A. J. Land surface temperature from Ka band (37 GHz) passive microwave observations. *J. Geophys. Res. Atmospheres* **114**, DOI: 10.1029/2008JD010257 (2009).

37. Rotenberg, E. & Yakir, D. Distinct patterns of changes in surface energy budget associated with forestation in the semiarid region. *Glob. change biology* **17**, 1536–1548 (2011).

38. Wilson, K. *et al.* Energy balance closure at fluxnet sites. *Agric. For. Meteorol.* **113**, 223–243 (2002).

39. Stoy, P. C. *et al.* A data-driven analysis of energy balance closure across fluxnet research sites: The role of landscape scale heterogeneity. *Agric. forest meteorology* **171**, 137–152 (2013).

40. Foken, T. The energy balance closure problem: an overview. *Ecol. Appl.* **18**, 1351–1367 (2008).

41. Chen, Y., Sun-Mack, S., Minnis, P., Smith, W. L. & Young, D. F. Surface spectral emissivity derived from modis data. In *Optical Remote Sensing of the Atmosphere and Clouds III*, vol. 4891, 361–369 (International Society for Optics and Photonics, 2003).

42. Juang, J.-Y., Katul, G., Siqueira, M., Stoy, P. & Novick, K. Separating the effects of albedo from eco-physiological changes on surface temperature along a successional chronosequence in the southeastern united states. *Geophys. Res. Lett.* **34** (2007).

43. Guillevic, P. *et al.* Land surface temperature product validation best practice protocol. version 1.1. *Best Pract. for Satell. Land Prod. Valid.* 60 (2018).

44. Mira, M., Valor, E., Boluda, R., Caselles, V. & Coll, C. Influence of soil water content on the thermal infrared emissivity of bare soils: Implication for land surface temperature determination. *J. Geophys. Res. Earth Surf.* **112** (2007).

45. Chen, C. Determining the leaf emissivity of three crops by infrared thermometry. *Sensors* **15**, 11387–11401 (2015).

46. Vishnevetsky, I., Rotenberg, E., Kribus, A. & Yakir, D. Method for accurate measurement of infrared emissivity for opaque low-reflectance materials. *Appl. optics* **58**, 4599–4609 (2019).

47. Eisenhauer, J. G. Regression through the origin. *Teach. statistics* **25**, 76–80 (2003).

48. Foken, T. *et al.* Post-field data quality control. In *Handbook of micrometeorology*, 181–208 (Springer, 2004).

49. Wan, Z. Collection-5 modis land surface temperature products users' guide. *ICESS, Univ. California, Santa Barbar.* (2007).

50. Delucchi, L. pymodis: from satellite to gis maps. In *FOSS4G 2014* (2014).

51. Bahir, M. *et al.* Evaluation and Aggregation Properties of Thermal Infra-Red-Based Evapotranspiration Algorithms from 100 m to the km Scale over a Semi-Arid Irrigated Agricultural Area. *Remote. Sens.* **9**, 1178, DOI: 10.3390/rs9111178 (2017).

52. Saltelli, A., Albrecht, D., Tarantola, S. & Ferretti, F. A new sample-based algorithms to compute the total sensitivity index. *arXiv preprint arXiv:1703.05799* (2017).

53. Jin, M. & Liang, S. An Improved Land Surface Emissivity Parameter for Land Surface Models Using Global Remote Sensing Observations. *J. Clim.* **19**, 2867–2881, DOI: 10.1175/JCLI3720.1 (2006).

5 Supplementary Information

SI1. Abbreviation list

Table 3. Abbreviation list

Symbol	Description	Unit
R_{net}	Net radiation	W m^{-2} m
H	Sensible heat flux	W m^{-2}
LE	Latent heat flux	W m^{-2}
G	Ground heat flux	W m^{-2}
R_{lem}	Emittied longwave radiation	W m^{-2}
ε	Surface emissivity	(-)
σ	Stefan-Boltzmann constant	W m^{-2}K^{-4}
T_s	Surface temerature	K
R_{sdwn}	Down-welling short-wave	W m^{-2}
R_{ldwn}	Down-welling long-wave	W m^{-2}
R_{sref}	Reflected shortwave	W m^{-2}
α	Surface albedo	(-)
m	Aerodynamic conductance to heat transport	(m/s)
ε 31	Spectral emissivity for wavelength of 11 μm	(-)
ε 32	Spectral emissivity for wavelength of 12 μm	(-)
BADAM	Ameriflux dataset	(-)
TERRA	NASA scientific research satellite	(-)
NATT	North Australian Tropical Transect	(-)

SI2. Comparison table of plot-scale LST with landscape LST using landscape and plot-scale ε
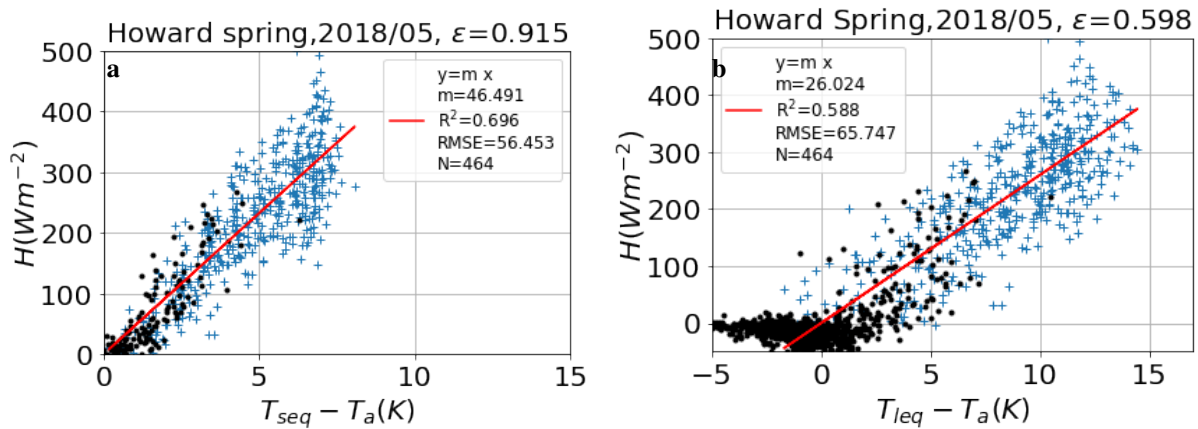
SI3. Emissivity estimation at Howards spring and positive $T_s - T_a$

Figure 8. H and ΔT plots at Howards Spring with optimised emissivity

| Sites | Landscape-scale ε | | | | | Plot-scale ε | | | | | |
| | ε | seq | | leq | | seq | | | leq | | |
		R^2	bias	R^2	bias	opt ε	R^2	bias	opt ε	R^2	bias
SP	0.974	0.80	-3.67	0.81	-4.61	0.96	0.81	-3.0	0.85	0.82	-1.91
AS	0.974	0.93	-4.78	0.93	-6.31	0.96	0.93	-3.4	0.82	0.93	-1.92
TT	0.974	0.55	-6.76	0.57	-8.30	0.95	0.58	-5.06	0.80	0.52	-4.02
HS	0.985	0.16	-8.89	0.16	-9.90	0.92	0.21	-4.78	0.6	0.22	-2.47
LF	0.985	0.40	-10.0	0.41	-11.0	0.92	0.40	-4.41	0.6	0.41	-2.57
AR	0.985	0.18	-2.61	0.27	-3.51	0.997	0.23	-2.93	0.96	0.252	-2.98
DU	0.985	0.80	-3.67	0.81	-4.61	0.99	0.428	-3.682	0.985	0.425	-3.926
TUM	0.983	0.82	-2.27	0.84	-2.10	0.99	0.89	0.99	0.97	0.89	1.93
BR	0.983	0.937	0.525	0.937	-0.195	0.98	0.917	1.87	0.82	0.895	2.72
YA	0.974	0.855	-2.081	0.855	-3.45	0.97	0.522	-4.517	0.93	0.793	-0.582

Table 4. Comparison of plot-scale LST with landscape-scale daytime LST (MODIS, MODA001) at TERRA daily time of pass. Plot scale LST is obtained using landscape-scale emissivity (MODIS ε) and plot-scale emissivity (Optimum ε) at study sites. The reported plot-scale emissivity are median values and landscape emissivity are MODIS based. Bias is defined as mean of $T_s - T_{MODIS}$, R^2 is coefficient of determination between plot-scale LST in comparison to landscape-scale LST. The site acronyms can be found in Table 2

SI4. T_s **sensitivity to** ε **at Alice spring and Tumbarumba**
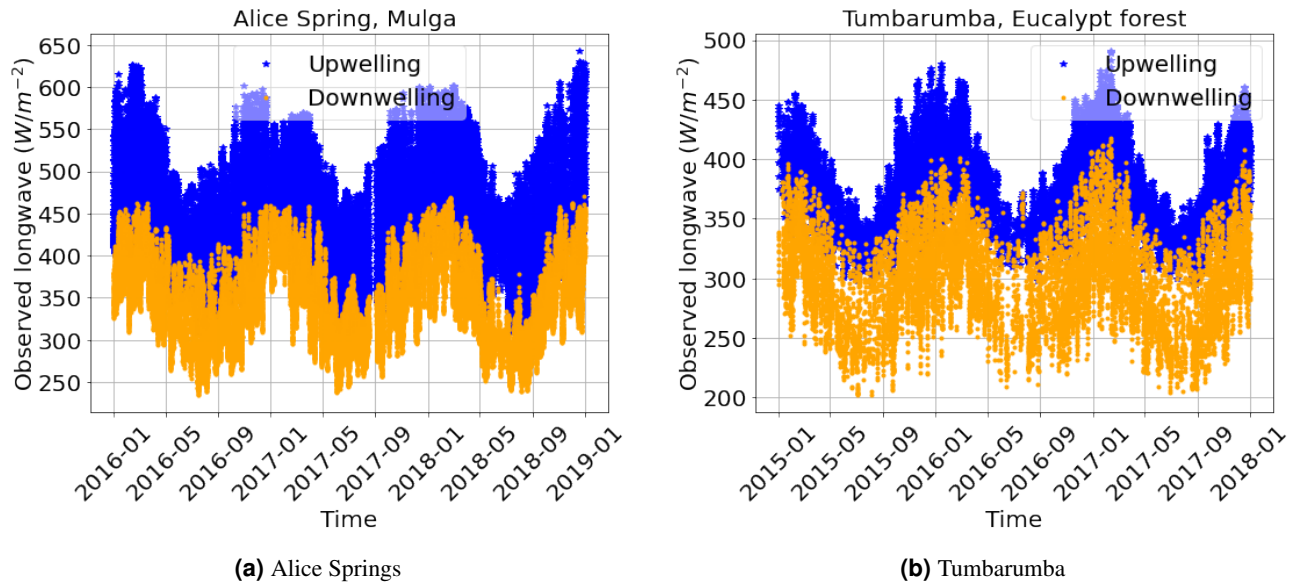

(a) Alice Springs **(b)** Tumbarumba

Figure 9. Measured up-welling and down-welling longwave timeseries

In general the broadband emissivity range for a land cover can vary between 0.87 to 0.98[53]. The noontime measured longwave for two contrasting landcover types (semi-arid mulga, tropical savanna woodland) are used to quantify the sensitivity of LST to emissivity as shown in Fig. (10).
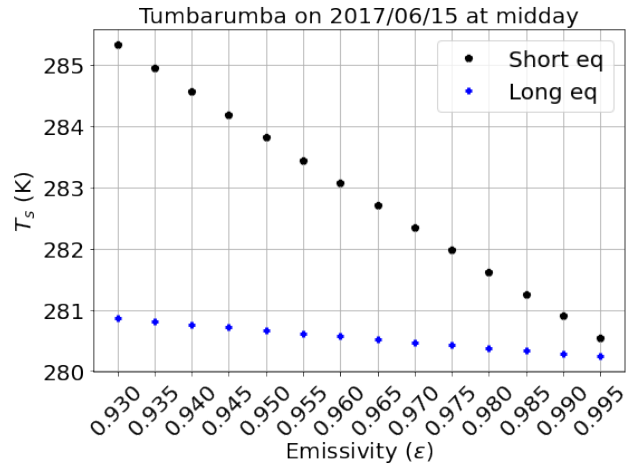
SI5.RMSE and Epsilon
SI6.Energy imbalance and observed fluxes
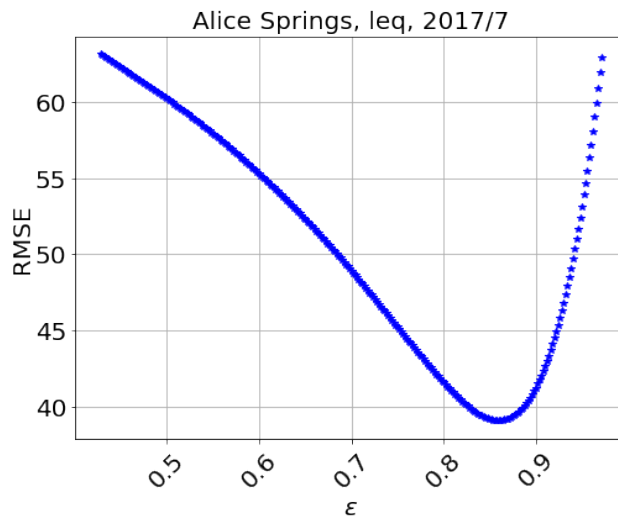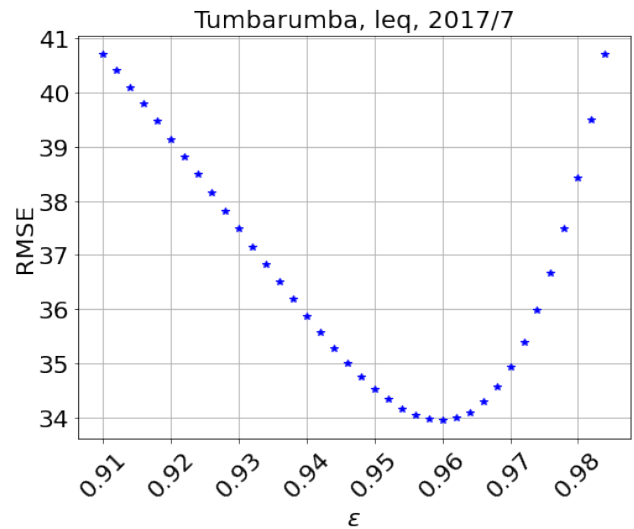**SI7.H and intercept**
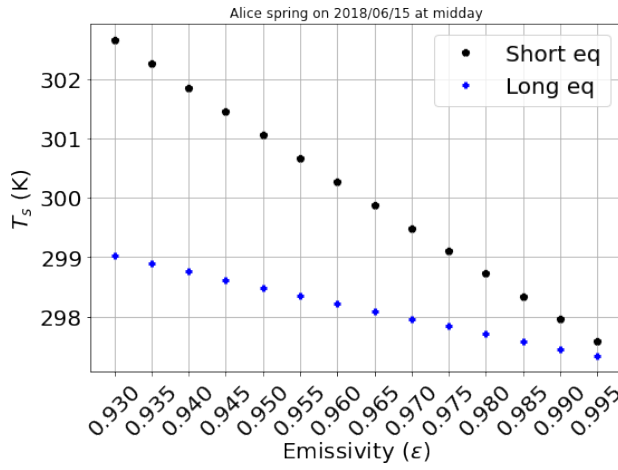
(a)

(b)

Figure 10. Sensitivity of LST estimated using two equations to the range of Broadband emissivity The black dots and blue Stars depicts LST using simplified (Eq. 11) and complete (Eq. (6). Midday longwave measurement for 15June, 2016 at Alice Springs and Tumbarumba is used

(a) Alice Springs

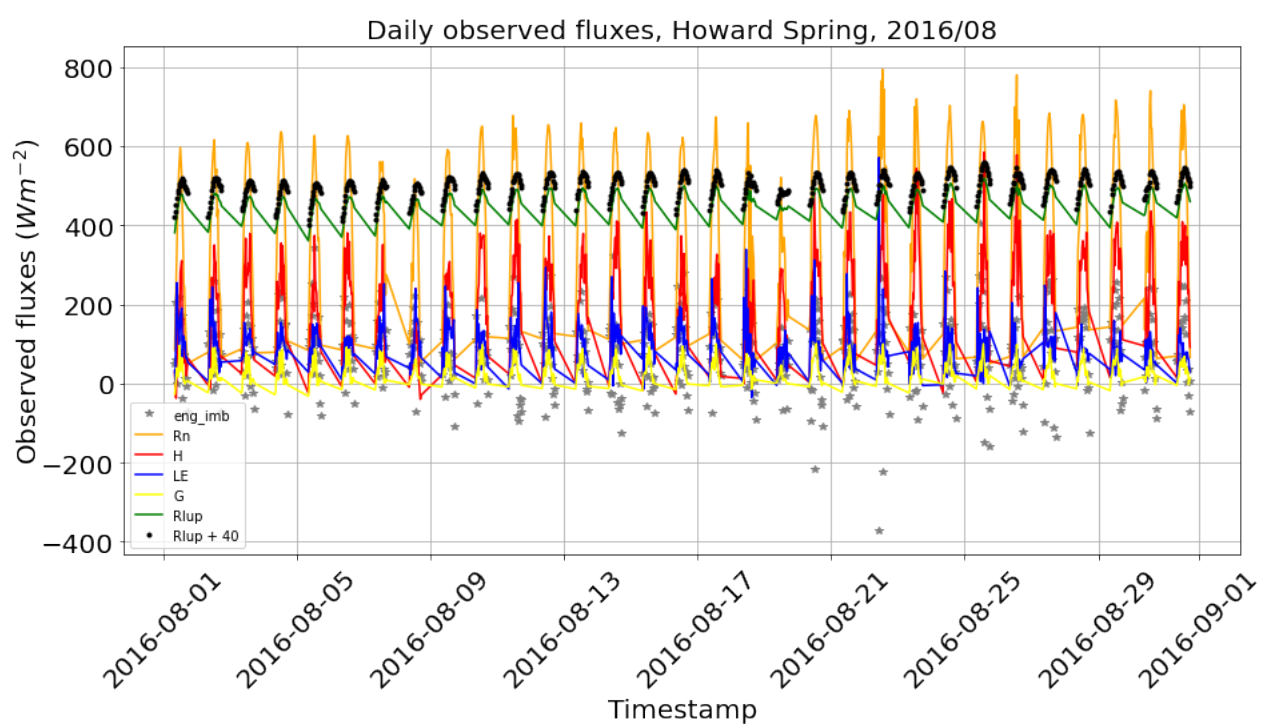**(b)** Tumbarumba

Figure 11. RMSE and emissivity curve

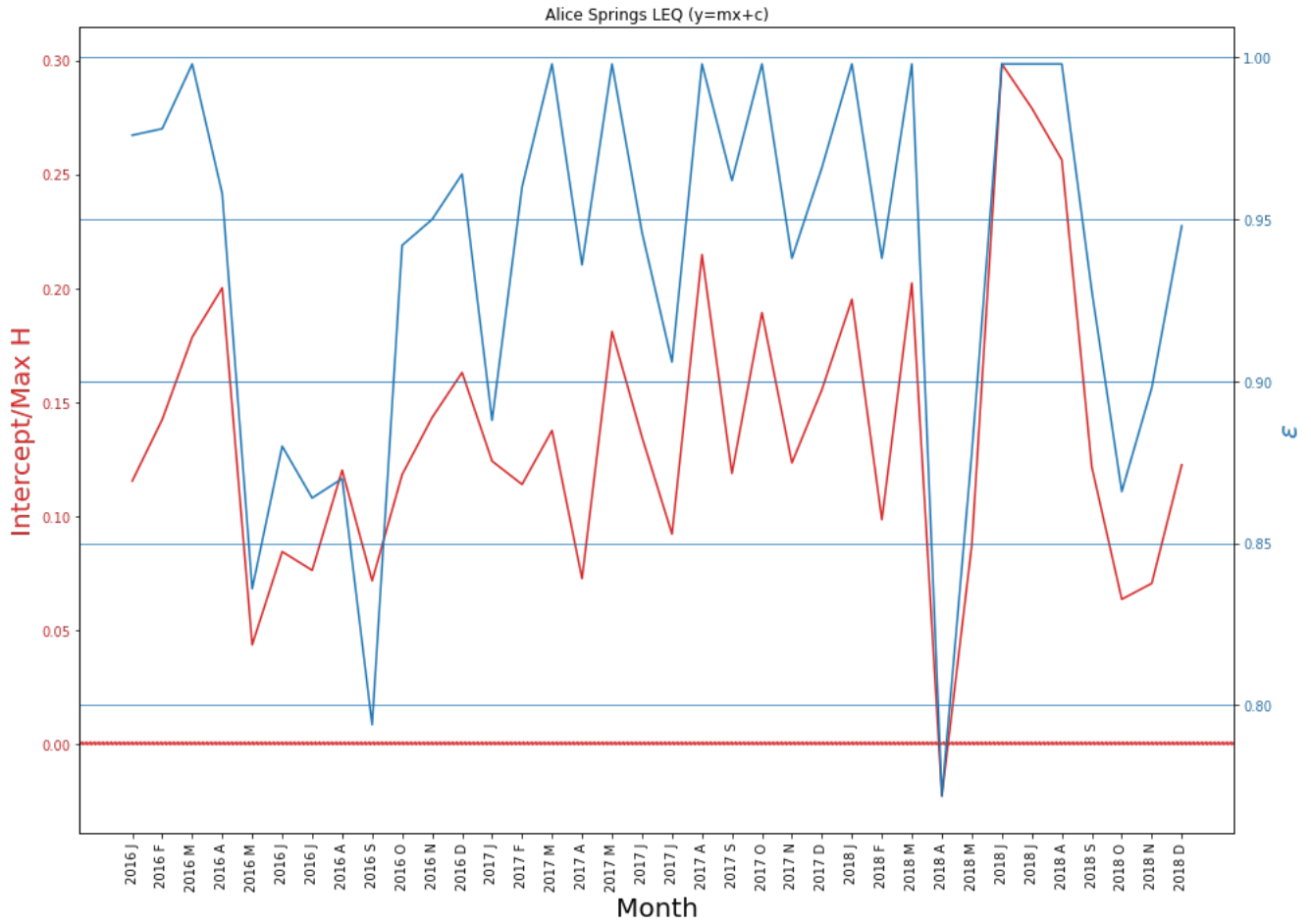**Figure 12.** Measured fluxes and estimated energy imbalance at Howard springs for 2016/08

Figure 13. Monthly H ΔT plots showing offset at ΔT=0 **(a)** using simplified equation (Eq. 11). **(b)** using complete equation (Eq. 6)(c). Estimated intercept (c)for each month using $H = m(T_s - T_a) + c$. Red line is intercept and blue line shows monthly ε obtained by minimising RMSE at Alice Springs (2016 - 2018).